THE AMERICAN SOCIETY OF MECHANICAL ENGINEERS
345 E. 47th St., New York, N.Y. 10017

95-GT-143

EXPERIMENTAL AND NUMERICAL INVESTIGATIONS OF AERODYNAMIC ASPECTS OF HOT GAS INGESTION IN ROTOR-STATOR SYSTEMS WITH SUPERIMPOSED COOLING MASS FLOW

Dieter Bohn, Erik Johann* and Uwe Krüger
Institute of Steam and Gas Turbines
Aachen University of Technology
Germany

* joined BMW-Rolls-Royce, Berlin in October 1994

ABSTRACT

Modern "High Temperature Gas Turbines" need very complex cooling configurations. Not only the turbine vanes and blades, but also the turbine discs, are cooled by air flow extracted from the compressor. Therefore, rotor-stator systems with a superimposed cooling mass flow are found in many constructions of gas turbines. The hot gas ingress into the wheelspace between stator and rotor, taking place under special conditions, is one of the major problems in these systems.

An experimental set-up has been built to get a better knowledge of the aerodynamics of such configurations. The ingress of hot gas into the wheelspace with different sealing configurations has been considered by the measurements of surface pressure and velocities (using the LDA-measurement technique) in the shrouded rotor-stator-system. A variable mainstream flow (Ma-number up to 0.7, Re-number up to $2 \cdot 10^6$) - with and without nozzle guide vanes - has been realized, to obtain flow situations approximating those in real gas turbines.

Parallel to the experiments, the flow structure has been calculated numerically using a modern multiblock finite-volume-scheme with non-orthogonal body-fitted grids. The influence of the mainstream flow has also been taken into account. Two different versions of the k-ε-turbulence model have been used to describe the turbulent effects of the flow.

Important features of the experimental results are as follows: hot gas ingress can not only occur on the stator but also on the rotor side of the wheelspace depending on the conditions between the cooling gas and the mainstream flow. In real systems with pressure and velocity gradients in the circumferential direction, hot gas ingestion can not be completely prevented. It was only in the 2-D-axisymmetric case, without guide nozzles in the mainstream, that hot gas ingress could be suppressed completely. The numerical data has been compared to the solution obtained by similitude theory as well as to the measurements. It was found that the data correspond reasonably well. The numerical results confirm the conclusions drawn by experiment about the physical mechanism of hot gas ingress into the wheelspace.

NOMENCLATURE

c_l		nozzle exit velocity
c_p		nondimensional static pressure coefficient
c_r		radial velocity
c_u		circumferential velocity
c_z		axial velocity
G	$= s/R$	rotor-stator gap ratio
G_c	$= s_c/R$	axial seal clearance ratio
h		height of nozzle guide vanes
h		enthalpy
m		mass flow rate
p		pressure
Δp		static pressure difference
r		radial coordinate
R		outer radius of stator
s		axial gap between rotor and stator
s_c		seal clearance
t		pitch
T		temperature
ΔT		temperature difference
Tu		turbulence intensity
z		axial coordinate
α		absolute flow angle referred to axial direction
β	$= c_u/\omega r$	relative rotation of core
β^*		β without superimposed mass flow (β for $c_w=0$)
κ		ration of specific heats (c_p/c_v)
φ		circumferential coordinate

Presented at the International Gas Turbine and Aeroengine Congress and Exposition
Houston, Texas - June 5-8, 1995

ξ	= r/R	nondimensional radial coordinate
ζ	= z/s	nondimensional axial coordinate
μ		dynamic viscosity
ρ		density
ω		angular speed of disc

Subscripts:

coolant	coolant flow
hot	mainstream flow
0	inlet of mainstream flow
1	outlet of mainstream flow
0	inlet of mainstream flow
LE	nozzle guide vanes
max	maximum
min	minimum
ref	reference
rez	recirculation

$c_w = \frac{\dot{m}_{coolant}}{\mu R}$ nondimensional coolant mass flow rate

$c_p = \frac{\Delta p_i}{\frac{\rho_1}{2} c_1^2}$ nondimensional static pressure coefficient

$Ma_{c1} = \frac{c_1}{\sqrt{\kappa R T_1}}$ external flow Mach number

$Re_\omega = \frac{\rho \omega R^2}{\mu}$ rotational Reynolds number

$Re_{c_1} = \frac{c_1 \rho_1 R}{\mu_1}$ external flow Reynolds number

$p^*(r) = \frac{p(r) - p_{hub}}{p_{hub}}$ nondimensional static pressure difference (mean value per pitch)

$\Delta p^*(r) = \frac{p_{max}(r) - p_{min}(r)}{p_{hub}}$ nondimensional static pressure difference (maximum difference value per pitch)

$\eta_{Kohl}(r) = \frac{T(r) - T_{hot}}{T_{coolant} - T_{hot}}$ cooling effectiveness (mean value per pitch)

$\Delta\eta_{Kohl}(r) = \frac{\Delta T_{max}(r)}{T_{coolant} - T_{hot}}$ cooling effectiveness (maximum difference value per pitch)

$\lambda_t = \frac{c_w}{(Re_\omega)^{0.8}}$ turbulent flow parameter

INTRODUCTION

In modern gas turbines up to 20% of the compressed air is bled off for cooling and sealing purposes. Approximately a quarter of this air is used for disc cooling and prevents the ingress of hot gas into the wheelspace between the stator and rotor. Figure 1 shows simplified diagrams of disc-cooling systems that are commonly used. A radial outflow of air is used both to cool the rotor disc and to stop the ingestion of hot mainstream flow past the seals.

Higher gas temperatures at the turbine inlet, with a simultaneous increase of the compressor pressure ratio, increase the thermal efficiency of gas turbines. But a large coolant mass flow suppresses this advantage and therefore the designer is faced with the problem of minimizing the coolant flow without reducing the life of the mechanically and thermally stressed parts

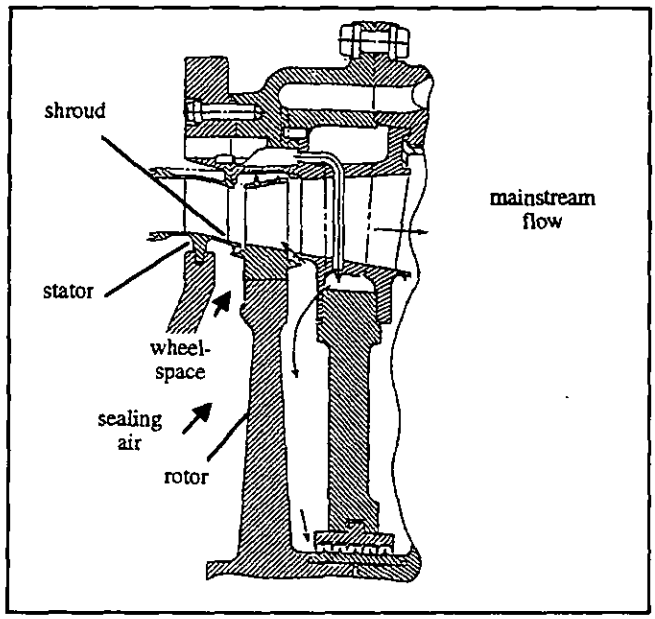

FIG. 1: WHEELSPACE IN A TURBINE ROTOR

of the gas turbine. In this paper, experimental and theoretical results are presented for an enhanced understanding of the phenomena affecting the ingestion. The paper is chiefly concerned with a comparsion between 2D and 3D effects from the LDA-measurements, with the numerical results in the 2D-case.

Bayley and Owen (1970) examined a shrouded rotor-stator system with a simple axial clearance seal. They were operating with no mainstream flow above the rim seal and they give a correlation for the minimum coolant flow rate necessary to prevent the ingress of hot gas. Phadke and Owen (1983) extended this correlation with a variety of radial clearance rim seals again in a test rig without mainstream flow. They showed that the minimum coolant flow was directly proportional to the rotational Reynolds number.

Bhavnani et al. (1992) have further examined the influence of disc pumping alone on the ingress for a double rim seal arrangement without mainstream flow. All these models are relevant if the rotational effects dominate the mainstream effects.

The influence of external flow has been noted by different workers. The experimental work of Abe et al. (1979) confirmed the importance of this effect under the presence of circumferential pressure variations. Other studies from Phadke and Owen (1988), Dadkhah et al. (1991) and Hamabe and Ishida (1992) have included the mainstream flow in the 2D case (without NGV's) with pressure asymmetry in the annulus and in the 3D case caused by guide vanes. Two important results are given by these works: firstly, the presence of an axisymmetric external flow tends to improve sealing, and secondly circumferential asymmetries promote the ingestion of hot gas. For a complete stage, guide vanes combined with rotor blades, Green and Turner (1992) found that the measured ingestion could be less than the ingestion with NGV's alone. It seems that the 3D unsteady effects reduce the ingress of hot gas. The following studies by Chew et al. (1994) showed for a stator-rotor system without blades that under

different circumferential pressure variations caused by a variation of the axial distance of the trailing edge, the measured sealing effectiveness was dependent on the static pressure downstream of the guide vanes. Theoretical investigations with CFD calculations are given by Ko et al. (1993), Chew et al. (1994) and Guo et al. (1994). These works have illuminated the presence of the gap recirculation zone located inward of the rim seal. No experimental measurements in this interacting zone are available to date.

At the Institute of Steam and Gas Turbines at the Technical University Aachen, experimental and theoretical investigations have been carried out into the influence of mainstream flow on the ingestion of hot gas into the wheelspace.

Analyzing the basic conservation equations of mass, momentum and energy (see below) it can be demonstrated that

$$c_w = f(Re_u, Re_{cl}, Ma_{cl}, c_p, \rho/\rho_1, geo) \quad (1)$$

The rotational Reynolds number (Re_u) characterizes the disc pumping effect. The mainstream Reynolds number (Re_{cl}) and the Mach number (Ma_{cl}) define the working condition of the model turbine. The static pressure coefficient characterizes circumferential pressure asymmetries in the annulus on the hub. The density ratio compared both the density of mainstream flow and coolant mass flow.

EXPERIMENTAL SETUP

Test Rig

A general cross-section of the test rig is shown in figure 2. The model turbine stage included a stator-rotor system without blades on the rotor disc. The model turbine operated with cold air (60°C) coming from a large compressor stage. The static pressure downstream of the stage was atmospheric. The mainstream flow goes up to $\dot{m}_{hotgas}$ = 6 kg/s, this leads to a maximum Mach number up to Ma_{cl} = 0.7 and because of the atmospheric exit of the stage to a maximum Reynolds' number of the mainstream flow up to $Re_{cl} = 2 \cdot 10^6$. The rotor without blades is driven by an electrical motor with a rotor speed up to 15.000 rpm. The central rotor-stator assembly was supported inside the mainstream annulus by aerodynamic struts upstream of the guide vanes and downstream of the rotor. An aerodynamic NACA-profile was used for these struts in order to prevent them influencing the profile wake. Measurements with total pressure probes in the first

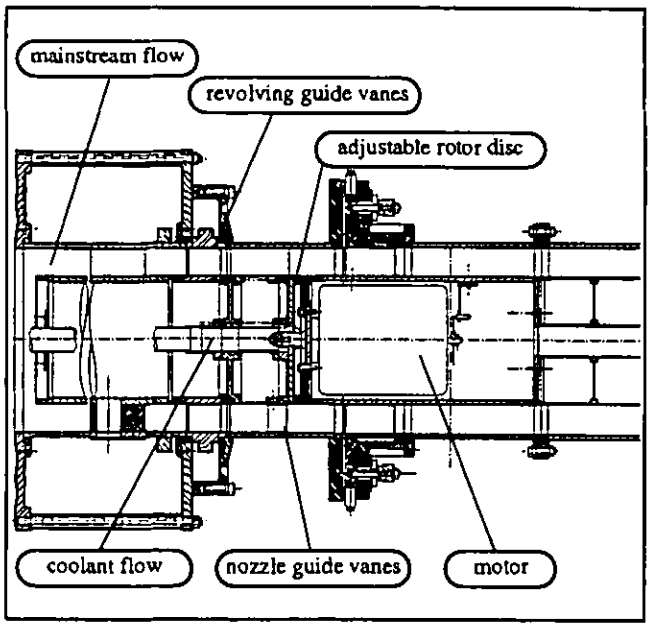

FIG. 2: CROSS SECTION OF THE TEST RIG

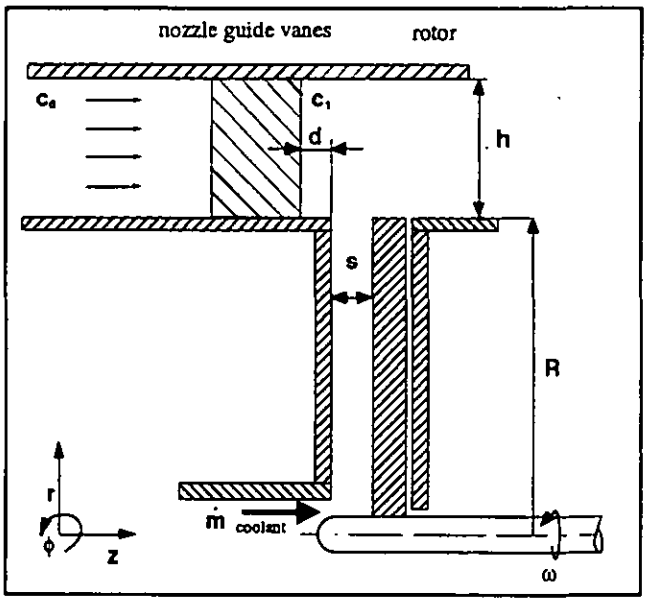

FIG. 3: CONFIGURATION 1 IS COMPOSED OF A PLANE STATOR COMBINED WITH A PLANE ROTOR DISC

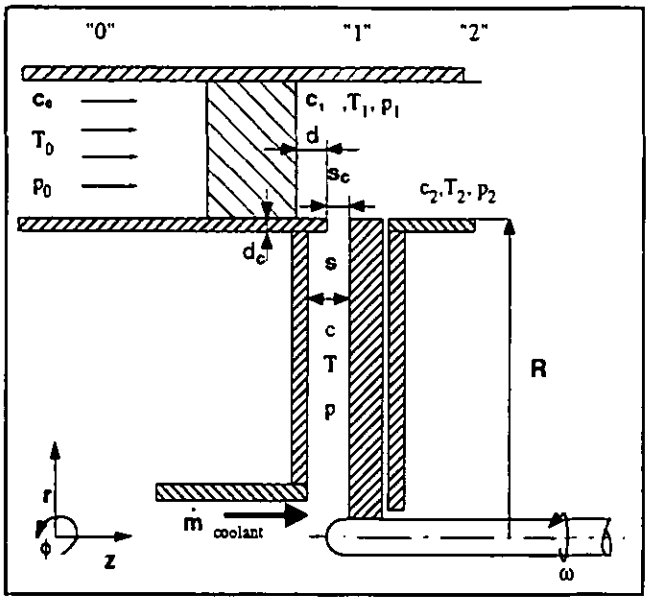

FIG. 4: CONFIGURATION 2 IS COMPOSED OF A STATOR WITH RIM SEAL COMBINED WITH A PLANE ROTOR DISC

revolving casing segment confirmed that, the following features are available:

- guide vanes and stator: traversable in the circumferential direction
- adjustable seal clearance
- adjustable eccentricity between rotor and stator
- adjustable non-parallel axes between rotor and stator

Two different geometries are investigated. Configuration 1 which is arranged as a flat stator combined with a flat rotor disc is shown in Figure 3. In this configuration, the seal clearance was maintained constant at s = 1.7 mm respectively G = 0.015. The hub diameter of both the stator and the rotor was 232.5 mm. The height of the guide vanes was h = 49 mm. The annulus had a constant diameter and contained 30 nozzle guide vanes (12° pitching).

Figure 4 shows configuration 2, where the flat rotor disc is combined with a rim seal on the edge of the stator. The thickness of this rim seal amounted to d_c = 4.5 mm. The rim seal clearance was adjusted to s_c = 0.6 mm respectively G_c = 0.005 and to s_c = 1.7 mm respectively G_c = 0.015 mm. The wheelspace gap amounted to s = 15.6 mm and s = 16.7 mm respectively G = 0.13 and G = 0.14. The guide vanes were mounted d = 3 mm upstream of the rim seal edge and the distance was maintained constant for all configurations. The coolant flow was supplied from a separate compressor and ranged up to $\dot{m}_{cool}$ = 0.03 kg/s. All mass flow rates, mainstream flow and sealing air were measured with calibrated orifice meters.

8 Fe-CuNi-thermocouples, 8 static pressure holes and 8 combined probes for total pressure and total temperature served for the determination of turbine inlet and outlet conditions. The online evaluation of the turbine measurements on the personal computer allowed adjustment and control of the working condition.

Pressure Measurements

About 80 holes (diameter 1.0 mm) for static pressure measurements were made in the wheelspace on one pitching at eight radius ratios. The innermost position was located at r/R = 0.46, the outermost at r/R = 0.972. A single circumferential row of static pressure taps in the mainstream is located 1.5 mm upstream of the edge of the seal and also 1.5 mm downstream of the trailing edge of the guide vanes. This served to measure the static pressure profile at the hub and corresponded with the static pressure in the interaction zone at r/R = 0.972. The pressures for the determination of turbine working conditions and the orifice meters were measured with calibrated single-pressure indicators. The pressures in the wheelspace and at the hub in the mainstream were measured with a calibrated pressure indicator using a personal computer controlled Scanivalve.

Velocity Measurements

For the measurement of the flow velocities and the turbulence intensity, a 2-D LDV-system with a 4 W Argon-Ion laser was available. The signals are detected by a two-component photomultiplier set-up with color separators and analyzed by a Burst Spectrum Analyser. The personal computer controlled the LDV-measurements.

Before entering the test section, both the coolant flow and the mainstream flow were seeded with oil droplets (particle size of about 1 µm). The optical access to the test section in the interacting zone between the mainstream flow and the coolant flow is realized by windows in the casing and in the stator disc.
Two different optical arrangements were used to measure the velocity components in the mainstream flow, in the interacting zone at the rim seal and by configuration 2 also in the inner wheelspace. The arrangement of the two fibre probes for quasi 3-D measurements in the mainstream flow and in the interacting zone is illustrated by figure 5. This optical setup allowed measurement of either circumferential and radial component of the flow field or the circumferential and axial component by changing the fibre plugs.

The arrangement of the fibre probe for 2-D measurements into the inner wheelspace is shown in Figure 6. A mounting for the

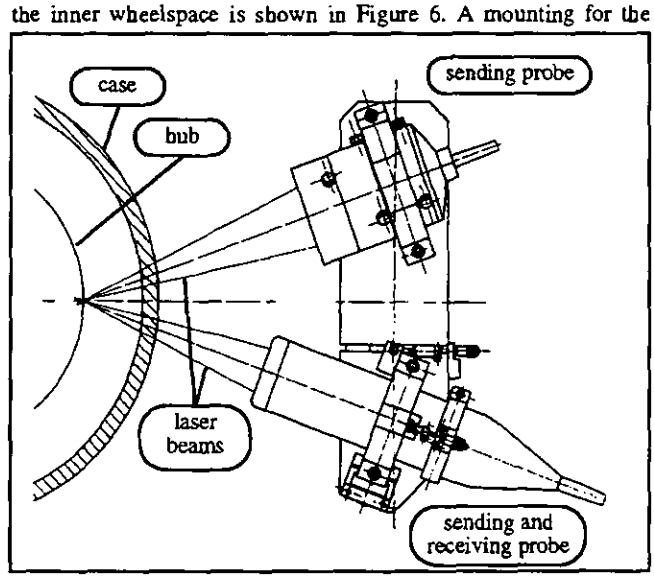

FIG. 5: QUASI 3D-LDA-MEASUREMENTS IN THE COOLANT-MAINSTREAM INTERACTION REGION

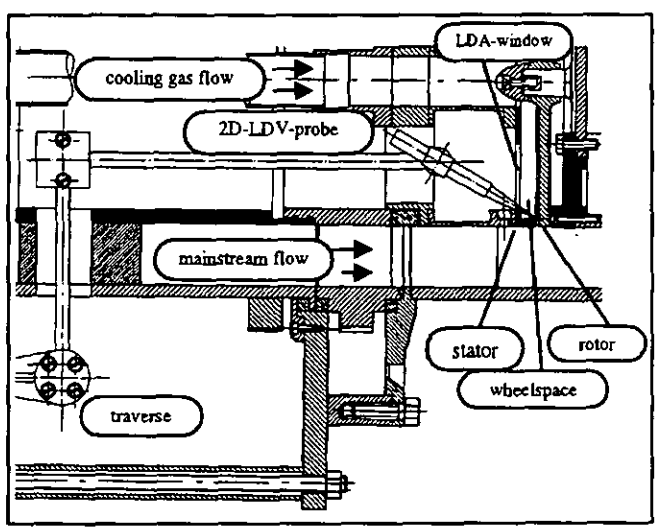

FIG. 6: DETAILS OF THE 2D-LDA-MEASUREMENTS INTO THE MACHINE

miniature 2-D fibre probe (diameter Ø 14 mm) was traversed in radial and axial coordinates by an external traverse table and the circumferential position could be changed by revolving the nozzle guide vanes.

EXPERIMENTAL RESULTS

Flow Field in the Coolant-Mainstream-Interaction Region without Vanes

For a better understanding of the 2-D and the 3-D effects in the flow field at the leading edge of the wheelspace, LDV-measurements have been made in the same rig without and with nozzle guide vanes. Figure 7 shows the measured circumferential and radial components of velocity at different radius positions in the wheelspace for $Re_{C1} = 0.46 \cdot 10^6$, $c_w = 1000$, $Re_u = 0.45 \cdot 10^6$, $G_c = 0.015$. The flow structure is highly turbulent. The boundary layers at the stator (z = 0 mm) and rotor side (z = 1.7 mm) have grown together. The circumferential component of velocity increases slightly over a wide range of the axial gap and increases sharply directly near the rotor surface (about 0.2 mm distance from the rotor). The radial variation of the measuring position shows hardly any influence on the velocity profiles. The circumferential velocity on the rotor disc was 58 m/s. The radial component of the velocity shows that the radial outflow is on the rotor at z = 1.7 mm and the ingestion of mainstream flow is near the stator. An eddy in the rim seal recirculation zone transports the mixed coolant-mainstream flow in the inner wheelspace and there the flow field is dominated by the inviscid rotating core. The ingested fluid runs along the stator in the direction of the machine axis. These results correspond well with the concentration measurements. In contrast to the computed 2-D results the stator side "suction effect" alone was measured. A very small eddy on the rotor side could not be found, which suggests that the

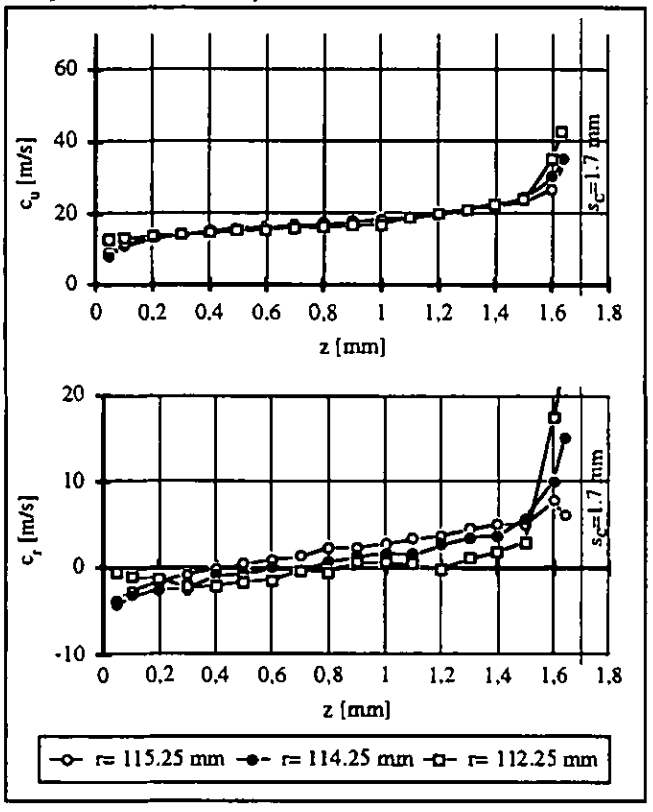

FIG. 7: CIRCUMFERENTIAL AND RADIAL VELOCITY IN THE WHEELSPACE NEAR THE RIM SEAL WITHOUT VANES, CONF.2, $Re_{C1}=0.46 \cdot 10^6$, $c_w=1000$, $Re_u=0.45 \cdot 10^6$, $G_c=0.015$

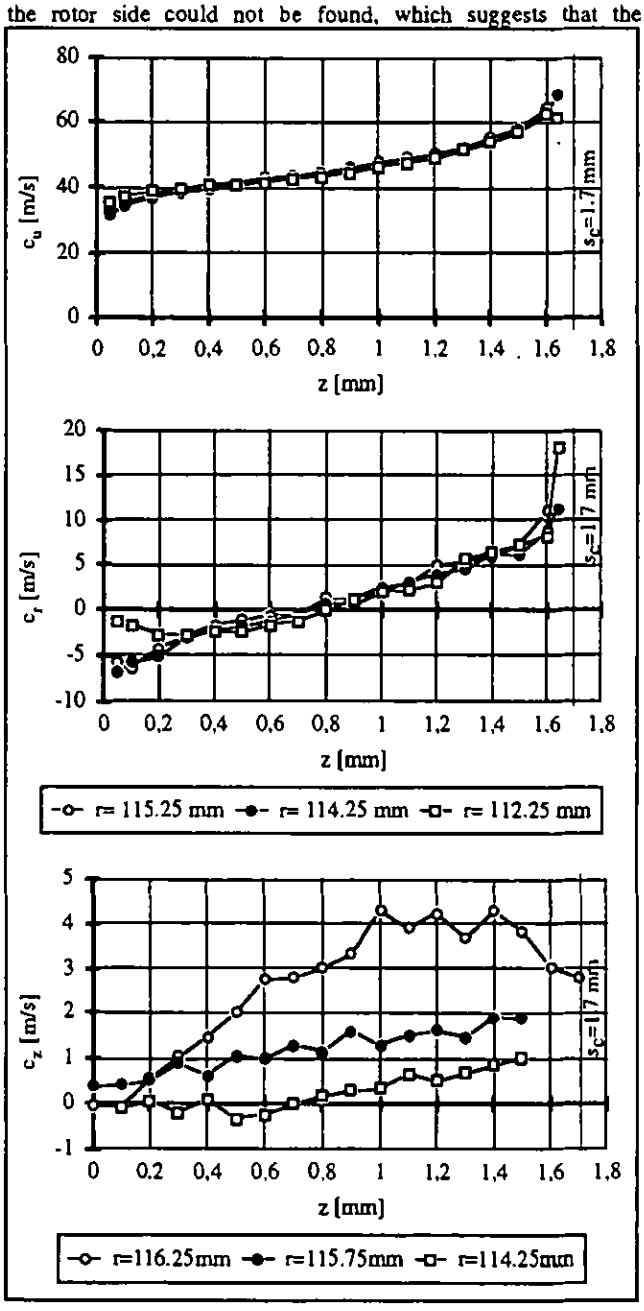

FIG. 8: CIRCUMFERENTIAL RADIAL AND AXIAL VELOCITY IN THE WHEELSPACE NEAR THE RIM SEAL WITHOUT VANES, CONF.2, $Re_{C1}=0.46 \cdot 10^6$, $c_w=1000$, $Re_u=1.13 \cdot 10^6$, $G_c=0.015$

boundary layer at the hub in the annulus has an important influence on the mechanism of the ingress. By variation of the rotational Reynolds number to $Re_u = 1.13 \cdot 10^6$ in figure 8, the circumferential component of the velocity increases proportional to the rotor speed. The rim seal recirculation zone also increases, which is shown by the radial velocity prnfile. On the one hand, the recirculation zone increases in the direction of the middle nf the gap width (z = 0.8) on the other hand, the level of radial velncity also increases on the stator side. In addition, the axial component of velocity is given in Figure 8. It shows the separation of the boundary layer of the mainstream flow at the leading edge of the wheelspace. Directly at the hub radius, the flow is speeded up over the gap width. At r = 114.25 mm at the stator, the axial velocity is negative, the flow ingress into the wheelspace is positive. Because of the disc pumping effect the axial components on the rotor side are also positive. But the level of axial velocity is very low and in the gap at r = 114.25 mm the flow structure seems to be 2-D. But measurements have shown that the turbulence structure is highly anisotropic in the axial direction.

Flow Field in the Coolant-Mainstream-Interaction Region with Guide Vanes

The influence of the nozzle guide vanes on the ingestion of mainstream flow is significant. The ingestion into the wheelspace increases as the nozzle guide vanes are moved closer to the rim seal. This is caused by the circumferential pressure distribution with high pressure differences per pitch. Figure 9 shows the static pressure cnefficient measured with static pressure tappings at varied positions from the guide vanes' trailing edge. For a significant effect of this 3-D mainstream flow on the ingestion, it is essential to mount the guide vanes near the rim seal. The distance between the trailing edge and the rim seal is d = 3 mm. The pressure measurements in figure 10 show that the mean value per pitch of the pressure is greater than zero in a wide range. Only in the case of $Re_u = 1.2 \cdot 10^6$ the pressure is less than zero at radial positions r/R less than 0.85. Near the rim section p* is greater than zero for

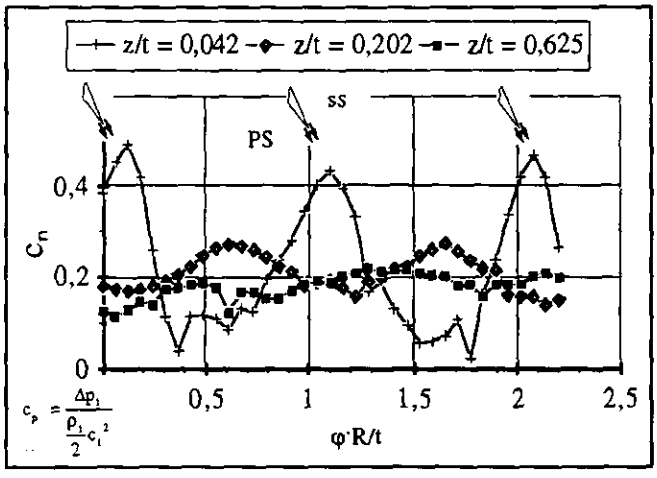

FIG. 9: PRESSURE COEFFICIENT AT DIFFERENT POSITIONS DOWNSTREAM OF THE TRAILING EDGE OF NOZZLE GUIDE VANES
($Ma_{c1}=0.787$; $Re_{c1}=1.9 \cdot 10^6$)

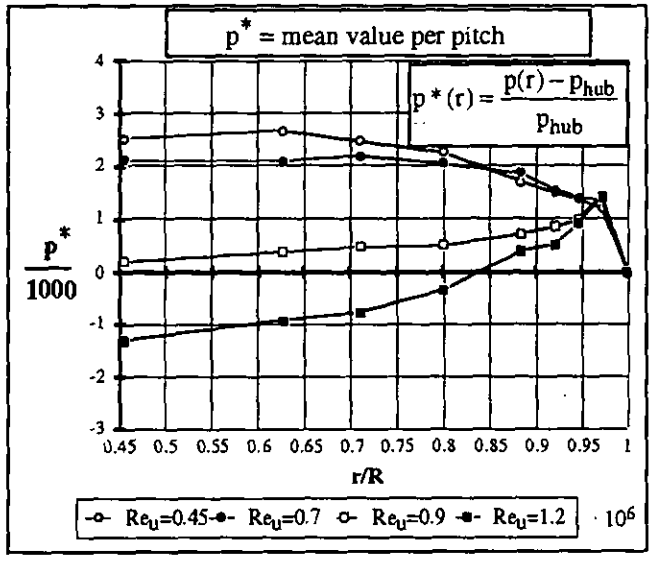

FIG. 10: NONDIMENSIONAL PRESSURE FOR CONFIGURATION 1
c_W=6500,s=1.7 mm, $Re_{c1}=0.74 \cdot 10^6$

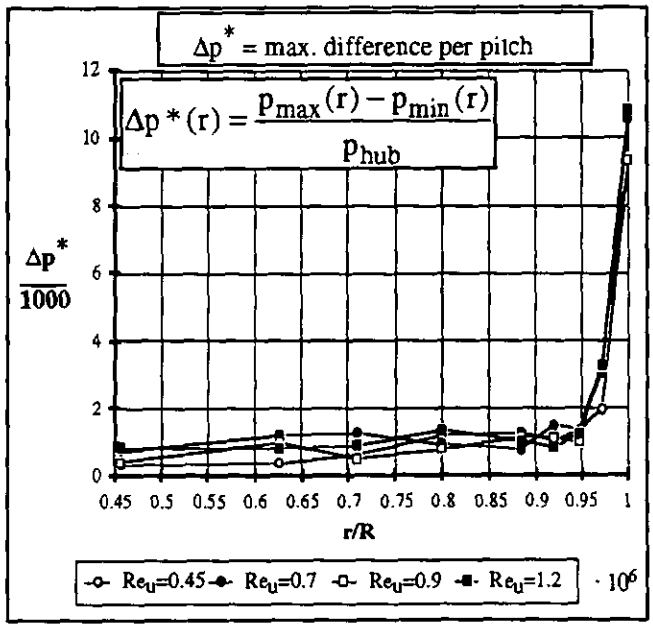

FIG. 11: MAIMUM PRESSURE DIFFERENCE FOR CONFIGURATION 1
c_W=6500,s=1.7 mm, $Re_{c1}=0.74 \cdot 10^6$

all Reynolds numbers. These measurements have been made by configuration 1. In comparison to the case without guide vanes, p* and Δp* was used to predict the ingress. If the pressure in the wheelspace is less than in the mainstream flow, then it is assumed that ingress occurs. If p* = 0 in the 2-D mainstream flow without guide vanes the criterion for sealing had been detected. Because of the high influence of the circumferential pressure distribution, in addition to the mean value of pressure, the maximum difference in

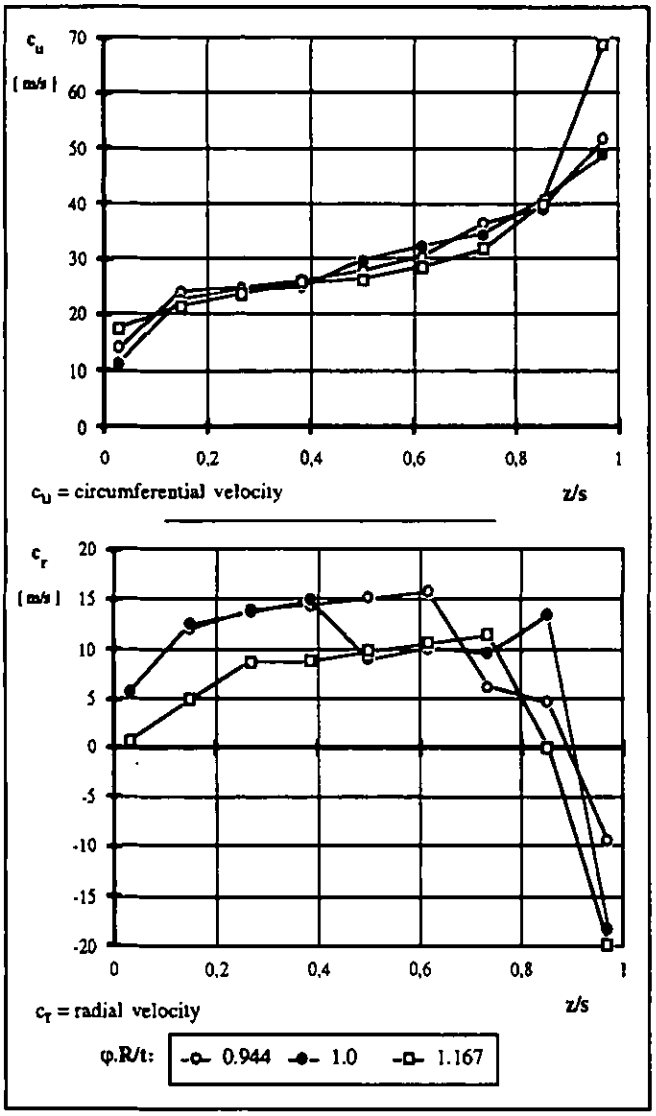

FIG. 12: CIRCUMFERENTIAL AND RADIAL VELOCITY IN THE WHEELSPACE WITH GUIDE VANES, CONF. 1
$Re_{c1}=0.74\cdot10^6$, $c_w=6680$, $Re_u=0.68\cdot10^6$, G=0.015

a pitch must be considered. In figure 11 the maximum difference values in a pitch are given. At the leading edge of the rim seal at r/R = 0.972 the effect of the mainstream pressure is significant. Although the mean value of pressure at r/R = 0.972 is postive, the addition nf the maximum difference pressure delivers a local pressure less than zero. This region is located in the wake of the guide vanes. Moreover, figure 11 shows that the pressure in the wheelspace decreases if the rotational Reynolds number increases. With it, the mixed coolant mainstream flow from the interaction reginn mnves powerfully into the wheelspace. The concentration measurements in the wheelspache which have been done in additinn tn the LDA-measurements confirmed this result. The maximum sealing effectiveness at r/R=0.972 was aboul 93%.

In additinn to the suction effect at the stator side, figure 12 shows the ingress of mainstream flow at the rotor side. This is

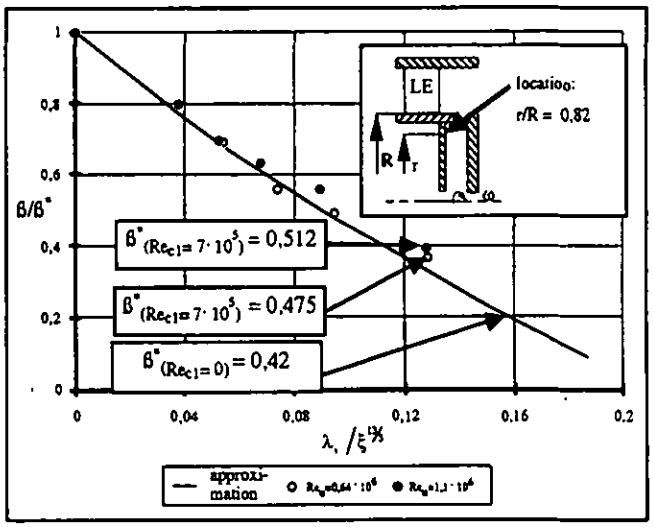

FIG. 13: THE VARIATION OF THE RELATIVE ROTATION OF THE CORE WITH RADIAL OUTFLOW AND MAINSTREAM FLOW WITH GUIDE VANES, CONF.2, G_c=0.005

caused by a very small change in the direction of the mainstream flow with the result that the boundary layer at the hub of the mainstream is turned into the wheelspace. The boundary layer downstram of the guide vanes is thinner than in the case without guide vanes. This corresponds well qualitatively with the computed effects. In the 3-D mainstream flow case, more coolant flow is needed for the same sealing effectivness and the maximum sealing effectiveness is less than in the 2-D case without vanes.

The variation of the relative rotation of the core in the inner wheelspace at the position r/R=0.82 for a rotor-stator system with outflow and mainstream flow is given by figure 13. The LDV-probe mounted in the model turbine was used for these measurements. The measurements show that the disc drags the core in the same manner as without mainstream flow if the relative rotation of core for c_w = 0 is known for different mainstream Reynolds numbers Re_{C1} and different rotational Reynolds numbers Re_u.

NUMERICAL INVESTIGATIONS

Numerical investigations of the complex flow situation described above have been carried out.

Basic Equations

The basic equations for prediction of the fluid flow in the wheelspace between rotor and stator are the conservation laws of cnntinuum mechanics, namely the continuity equation (2), the momentum equation (3) and the energy equation (4).
In common tensor form, these equations read:

$$\nabla\cdot(\rho\vec{v}) = 0 \tag{2}$$

$$\nabla\cdot(\rho\vec{v}\otimes\vec{v}) - \nabla\cdot(\mu_{eff}\nabla\vec{v}) = -\nabla\left(p+\frac{2}{3}k\right) + \nabla\cdot\left(\mu_{eff}(\nabla\vec{v})^T\right) \tag{3}$$

$$\nabla\cdot(\rho\vec{v}h_t) - \nabla\cdot\left(\frac{\lambda}{c_p}+\frac{\mu_t}{Pr_t}\right)\nabla h_t = 0 \tag{4}$$

Some important assumptions should be mentioned in this regard. The equations are valid for a compressible but steady-state flow. All primitive variables are density-weighted averaged variables (Favre-averaging). A fixed cylindrical coordinate-system (z,r,φ) has been used, in which r=0 identifies the axis. In this system the Nabla-operator becomes: $\nabla = \partial/\partial z + \partial/\partial r + 1/r\,\partial/\partial\varphi$. It has been carried out 2-D calculations, that means the derivatives $\partial/\partial\varphi$ has been neglected, while the circumferential velocity has still been considered.

Turbulence effects

The eddy viscosity hypothesis has been used to take turbulence effects into account, so the effective viscosity μ_{eff} is the sum of the laminar viscosity μ and the turbulent viscosity μ_t. Two additional equations for the turbulent energy k (5) and the dissipation rate ε (6) have to be solved to calculate the turbulent viscosity which is not a fluid property, but depends on the flow field. Depending on the turbulence model used, these equations read for the standard k-ε-model (5a, 6a and 7a):

$$\nabla\cdot(\rho\vec{v}k) - \nabla\cdot\left(\left(\mu + \frac{\mu_t}{Pr_{t,k}}\right)\nabla k\right) = \mu_{eff}\nabla\vec{v}\cdot\left(\nabla\vec{v} + (\nabla\vec{v})^T\right) - 2/3\,\nabla\cdot\vec{v}\left(\mu_{eff}\nabla\cdot\vec{v} + \rho k\right) - \rho\varepsilon \tag{5a}$$

$$\nabla\cdot(\rho\vec{v}\varepsilon) - \nabla\cdot\left(\left(\mu + \frac{\mu_t}{Pr_{t,\varepsilon}}\right)\nabla\varepsilon\right) = C_1\frac{\varepsilon}{k}\cdot\begin{pmatrix}\mu_{eff}\nabla\vec{v}\cdot\left(\nabla\vec{v} + (\nabla\vec{v})^T\right)\\ -2/3\,\nabla\cdot\vec{v}\left(\mu_{eff}\nabla\cdot\vec{v} + \rho k\right)\end{pmatrix} - C_2\rho\frac{\varepsilon^2}{k} \tag{6a}$$

$$\mu_t = C_\mu\rho\frac{k^2}{\varepsilon} \tag{7a}$$

and for the low-Reynolds-version of Launder and Sharma (1974) (5b, 6b and 7b):

$$\nabla\cdot(\rho\vec{v}k) - \nabla\cdot\left(\left(\mu + \frac{\mu_t}{Pr_{t,k}}\right)\nabla k\right) = \mu_{eff}\nabla\vec{v}\cdot\left(\nabla\vec{v} + (\nabla\vec{v})^T\right) - 2/3\,\nabla\cdot\vec{v}\left(\mu_{eff}\nabla\cdot\vec{v} + \rho k\right) - \rho\varepsilon - 2\mu\left(\nabla k^{\frac{1}{2}}\right)^2 \tag{5b}$$

$$\nabla\cdot(\rho\vec{v}\varepsilon) - \nabla\cdot\left(\left(\mu + \frac{\mu_t}{Pr_{t,\varepsilon}}\right)\nabla\varepsilon\right) = C_1\frac{\varepsilon}{k}\cdot\begin{pmatrix}\mu_{eff}\nabla\vec{v}\cdot\left(\nabla\vec{v} + (\nabla\vec{v})^T\right)\\ -2/3\,\nabla\cdot\vec{v}\left(\mu_{eff}\nabla\cdot\vec{v} + \rho k\right)\end{pmatrix} - C_2 f_2\rho\frac{\varepsilon^2}{k} + 2\frac{\mu\mu_t}{\rho}(\nabla\nabla\vec{v})^2 \tag{6b}$$

$$\mu_t = C_\mu f_\mu\rho\frac{k^2}{\varepsilon} \tag{7b}$$

The model involves a damping of the effective viscosity (7b) when the local turbulent Re number is low. Also the source terms of the k and ε equation are modified. The empirical functions fμ and f_2 are defined by:

$$f_\mu = \exp\left(\frac{-3.4}{\left(1 + 0.02\,Re_t\right)^2}\right) \tag{8}$$

$$f_2 = 1 - 0.3\exp\left(-Re_t^2\right) \tag{9}$$

where the local turbulent Reynolds number is given by:

$$Re_t = \frac{\rho k^2}{\mu\varepsilon} \tag{10}$$

The Launder-Sharma model is used because it allows the calculation of μ_t without knowledge of the grid distance from the walls. As a result no problems occur in corner regions of the flow domain. In this model there is no restriction of the range of the Reynolds number since this model is well adpated to both transitional flows and fully turbulent ones. Both are important features for the application in rotor-stator systems.

It is well known, for example see Chew 1984, that the standard k-ε-model is not well suited to high swirling flows as occur in the wheelspace. Therefore the model has been improved by the Richardson-correction. The turbulence damping effect of the swirl is taken into account by this well proven correction (Launder et al. 1977, Srinivasan et al. 1980 or Sloan et al. 1986) with a modification of the second source term of the ε-equation (6). This source term becomes:

$$-C_2\rho\frac{\varepsilon^2}{k}\left(1 - \frac{1}{1 + C_g Ri}\right) \tag{11}$$

Ri is the dimensionless gradient Richardson number (Launder et al. 1977):

$$Ri = \left(\frac{k}{\varepsilon}\right)^2\frac{w}{r}\left(\frac{1}{r}\frac{\partial(wr)}{\partial r}\right) \tag{12}$$

In addition, some more empirical constants appear in both turbulent models:

$Pr_{t,h}$	$Pr_{t,k}$	$Pr_{t,\varepsilon}$	C_1	C_2	C_μ	C_g
0.9	1.0	1.217	1.44	1.92	0.09	0.05

TAB. 1: CONSTANTS OF THE k-ε TURBULENCE MODEL

The set of equations is closed by the ideal gas law. Hence the Mach number is less than 0.3, variations in the pressure are ignored for the calculation of the density:

$$\rho = \frac{p_{Ref}}{R_{air}T} \tag{13}$$

This assumption is often called the weakly compressible flow option.

Numerical Scheme

A modern fully implicit Finite-Volume scheme with multi block technique and body fitted grid option has been used for solving the coupled set of partial differential equations (2-6) numerically. The SIMPLEC pressure-correction (Van Doormal and Raithby 1984) algorithm is adapted on a non-staggered grid, while avoiding the chequerboard oscillations by using the improved Rhie-Chow interpolation method (Rhie 1981 and Rhie and Chow 1983). For the diffusion terms a central differencing scheme is used, while the advection terms are discretised by

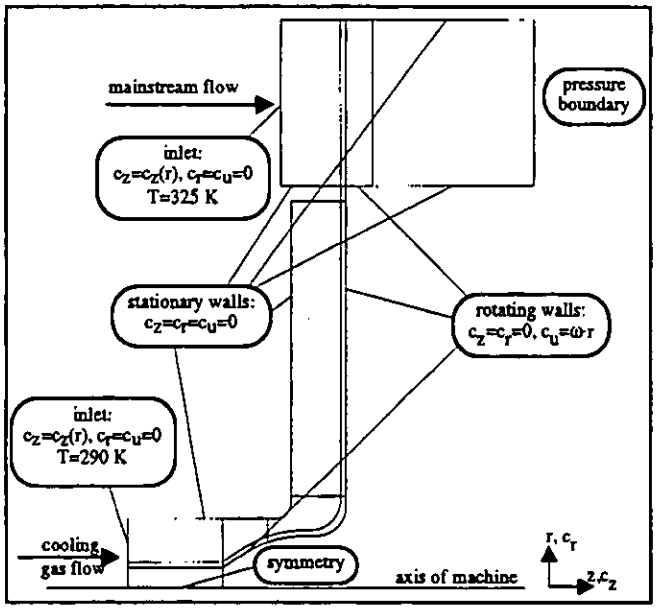

FIG. 14: COMPUTED DOMAIN OF THE WHEELSPACE WITH MAINSTREAM

hybrid differencing in which central differencing is used if the mesh Peclet number is less than 2, and upwind differencing, if the mesh Peclet number is greater than 2.

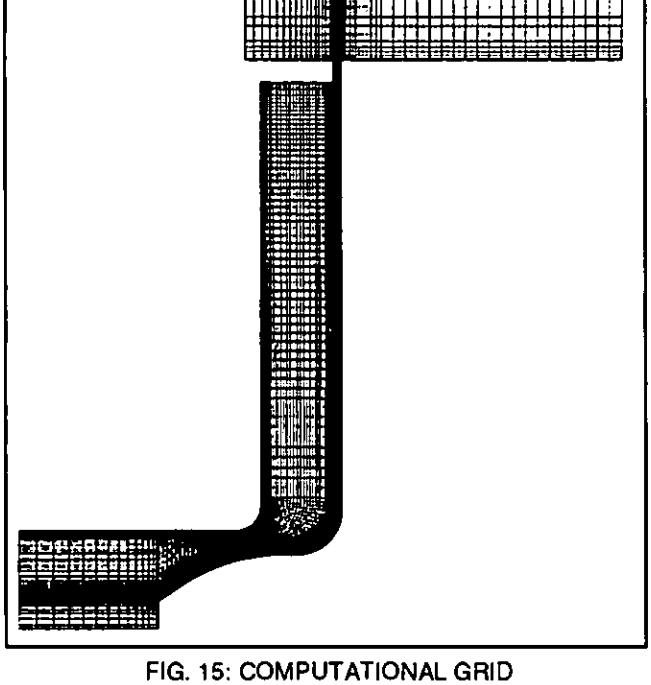

FIG. 15: COMPUTATIONAL GRID

Boundaries and Mesh

In figure 14, the geometry of the computed domain of configuration 2 is shown. The physical space is built up of 14 blocks. At the inlet boundaries a velocity profile in the radial direction has been given, while the axial and the circumferential velocities are zero. The temperature of the inflow into the wheelspace is 290 K and the temperature of the mainstream is 325 K. The turbulence intensity is assumed to be 2% at all inlets. All walls have zero velocities, with the exception of those on the rotor side which have a circumferential velocity w of ωr. All walls are assumed to be adiabatic. The rotational Re number is $1.13 \cdot 10^6$ and the Ma-number of the mainstream flow is 0.18.

Figure 15 shows the structured grid which is used for the calculation. The whole mesh consists of 10,075 grid nodes; the domain between rotor and stator contains 7,825 grid nodes. The large amount of grid points near the walls gives a very good resolution of the boundary layers.

NUMERICAL RESULTS

Before presenting some results of the complex flow configuration mentioned above, some attention should be paid to code-validation.

Code Validation

Two basic cases have been investigated: (i) the laminar fluid

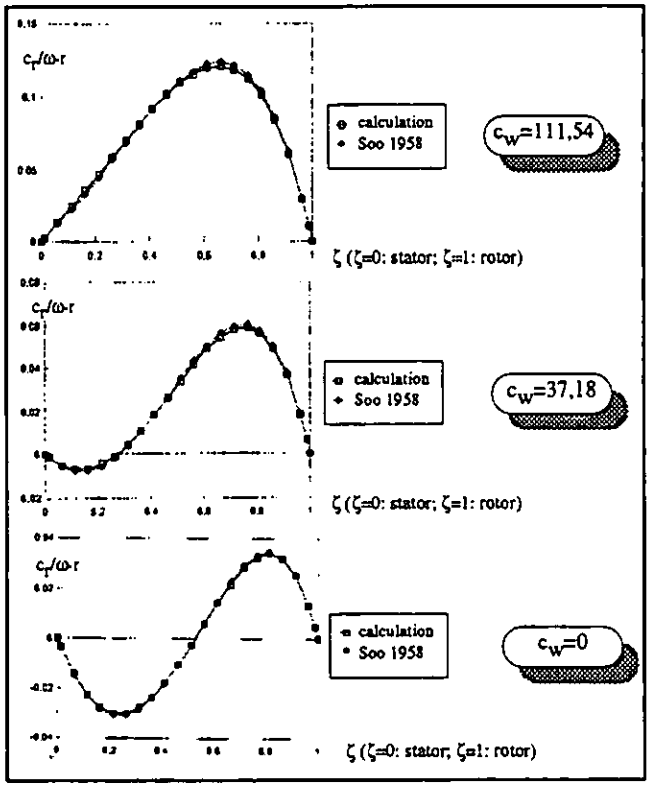

FIG. 16: COMPARISON OF THE RADIAL VELOCITY COMPONENT (ROTOR-STATOR) TO THE SOLUTION OF SOO (1958) FOR $Re=1.9 \cdot 10^4$ AND r/R=0.92

flow in very simple rotor-stator-systems which can be compared to the similitude solution given by Soo and Princeton 1958, the turbulent flow in a rotor-stator system with overlapping boundary layers which can be compared to the analytical solution given by Dorfman.

In figure 16, a comparison between the calculated radial velocity distributions and the distributions of Soo (similtude solution) for different mass flow parameters c_w are given. The numerical data fits the similtude solution very well. The highest difference is about 4%.

Also in the turbulent case of boundary layers growing together the numerical results, especially the core rotation, correspond sufficently well with the analytical data given by Dorfman.

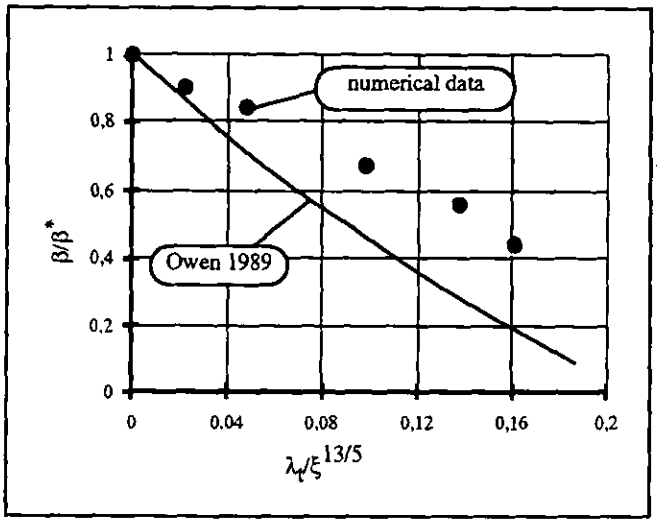

FIG. 17: COMPARISON BETWEEN NUMERICAL AND ANALYTICAL DATA

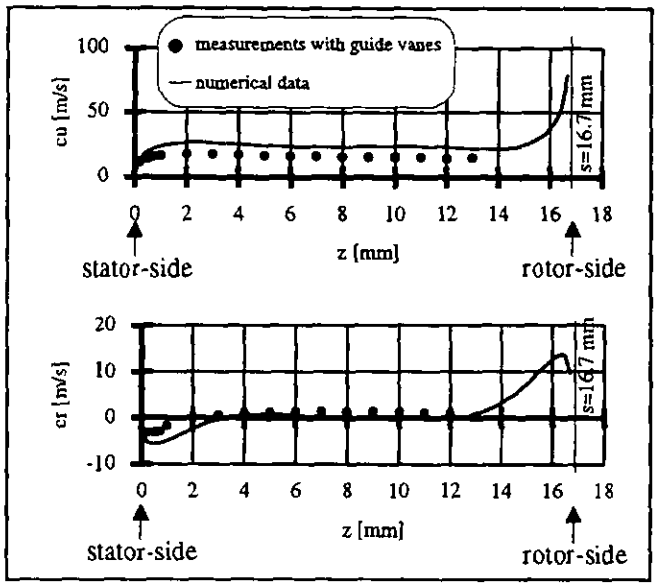

FIG. 18: CIRCUMFERENTIAL VELOCITY COMPONENT
C_W=6300, Re_u=1.0·10^6, Ma=0.31,ξ=0.815

Numerical Data

A comparison between the analytical solution of Owen and the numerical data for the core rotation of a rotor-stator-system with turbulent but separated boundary layers is given in figure 17. The cis qualitatively given by the numerics, but the values of the predicted core rotation are too high, which indicates that the damping effect of the superimposed mass flow is underestimated by the turbulence model, although the Richardson correction is used.

If the low-Reynolds number turbulent model (Launder-Sharma) is used, the core rotation is predicted too low also in the case of c_w=0.

For a radial position of ξ=r/R=0.815, the results of the numerical prediction are compared to the LDV-measurements in figure 18. The results correspond well qualitatively. As expected, the circumferential velocity and the radial velocity are overestimated by the numerical scheme. The reason for this is given above: the k-ε turbulence mndel predicts too much turbulence in the core region of the rotor-stator system. Figure 19 compares the turbulence energy predicted with the measured one. It is shown that the measured values of k are lower over the whole gap. In the diagramm on the right of figure 19 a section in the core region is shown. It can be demnnstrated that the k-ε-model with the Richardson correction works in the correct manner, this means the turbulence decreases. But in comparison to the experimental data this effect is not strong enough to decrease the swirl component in the core region. Maybe some modifications in the Richardson corrections will overrule that problem.

The qualitative flow structure, especially the interaction

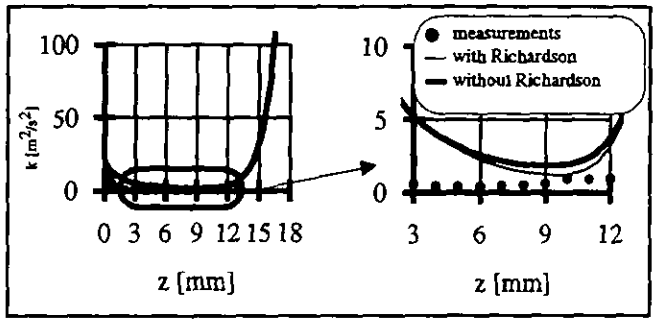

FIG. 19: TURBULENCE ENERGY k
C_W=6300, Re_u=1.0.10^6, Ma=0.31,ξ=0.815

between coolant and mainstream flow can be calculated with the numerical scheme sophisticatedly. In figure 20, the fluid flow at the coolant flow exit is shown for three different mass flow paramters c_W. As the experiments show, hoi gas ingestion occurs on the rotor side of the wheelspace, if c_W is not large enough. For the highest c_w value of 5062 no hot gas ingress occurs. As discussed above this 100% sealing effectiveness is only valid for the 2-D case without guide vanes, i. e. without a circumferential pressure gradient.

Future work on the numerical side will have to do both: first to improve the turbulence modelling and second to do 3-D calculations to include the circumferential pressure gradients.

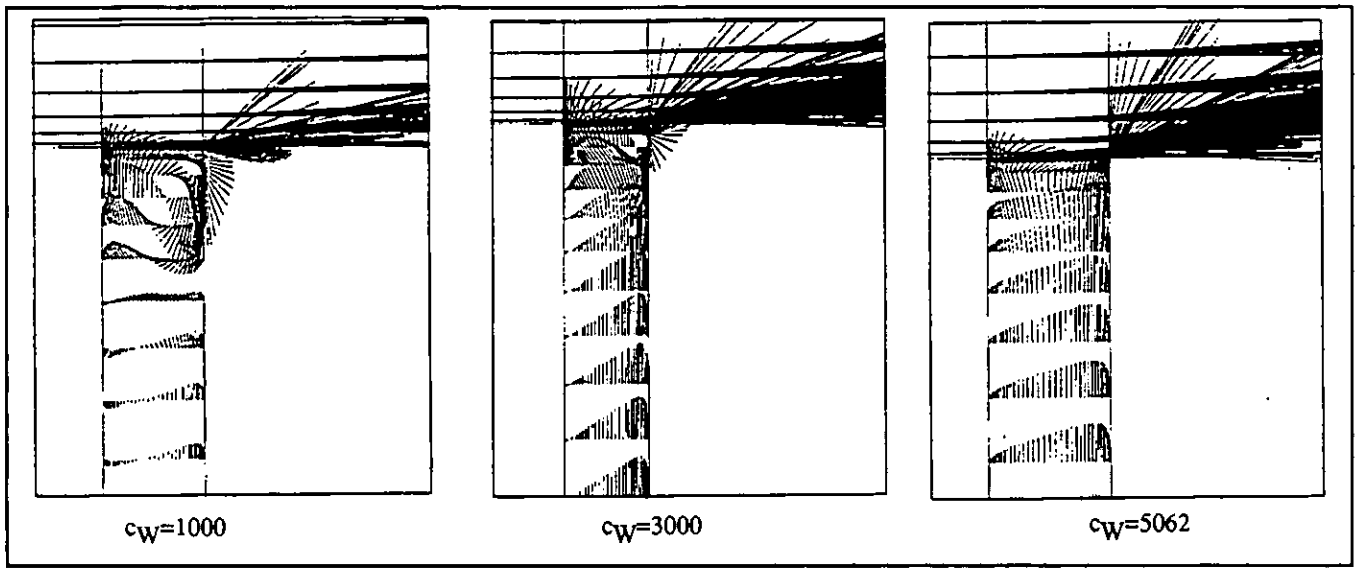

FIG. 20: FLOW PATTERN AT THE COOLANT FLOW EXIT $Re_u=1.0 \cdot 10^6$, Ma=0.31

SUMMARY AND CONCLUSIONS

Experimental and numerical investigations of the flow pattern in a rotor-stator-system with superimposed cooling mass flow have been carried out. A major aspect of the study has been the interaction of the coolant mass flow with the mainstream flow (hot gas ingestion).

With the experimental test rig considerations of hot gas ingress into the wheelspace with different sealing configurations has been done by measuring the surface pressure and velocities (LDA-measurement technique) under conditions similar to those in real gas turbines. In addition, numerical investigations of this very complex flow pattern have been carried out.

Experimentally it has been found that hot gas ingress can occur not only on the stator but also on the rotor side of the wheelspace. Only in the 2-D case, i. e. without guide vanes, a sealing effectiveness of 100% can be reached if the coolant mass flow through the wheelspace is large enough. In real systems with circumferential pressure gradients hot gas ingestion can not be prevented completely.

The numerical data has been found to correspond qualitatively well with the experiments. The turbulence intensity is overestimated by the k-ε turbulence model used, although a Richardson correction has been used. This correction works in the right direction but the effect is not large enough.

Future experimental work should work out the influence of the rotor blades on the hot gas ingress. The numerical work should focus on the improvement of the turbulence modelling and on the calculations of 3-D systems with a circumferential pressure gradient.

ACKNOWLEGEMENTS

The experimental part of this work was supported by the "Forschungsvereinigung Verbrennungskraftmaschinen e.V." (FVV).

REFERENCES

Bayley, F.J., Owen, J.M. (1970):
"The Fluid Dynamics of a Shrouded Disc System with a Radial Outflow of Coolant" J. of Eng. Power, Vo.92, p.35, 1970

Phadke, U.P., Owen, J.M.
"An Investigatinn of Ingress for an "Air Cooled " Shrouded Rotating Disk System With Radial- Clearance Seals" J. of Eng. Power, Vo.105, p.178, Hemisphere, Washington, 1983

Bhavnani, S.H., Khilnani, V.I., Tsai, L.-C., Khodadadi, J.M., Goodling, J.S.
"Effective Sealing of a Disk Cavity Using a Double-Toothed Rim Seal", ASME-Paper No. 92-GT-379, 1992

Abe, T., Kikuchi, J., Takeuchi, H.
"An Investigation of Turbine Disk Cooling (Experimental Investigation and Observation of Hot Gas Flow into a Wheelspace)" 13th CIMAC Conf., Vienna, Paper No. GT-30, 1979

Phadke, U.P., Owen, J.M.
"Aerodynamic Aspects of the Sealing of Gas Turbine Rotor-Stator Systems. Part 2:The Performance of Simple Seals in an Quasi-Axissymmetric External Flow" Int. J. of Heat and Fluid Flow, Vol. 9, No. 2, pp. 106-112, 1988

Dadkhah, S., Turner, A.B., Chew, J.W.
"Performance of Radial Clearance Rim Seals in Upstream Rotor-Stator Wheelspaces" ASME-Paper No. 91-GT-32, 1991

Hamabe, K., Ishida, K.
"Rim Seal Experiments and Analysis of a Rotor-Stator System with Nonaxissymmetric Main Flow" ASME-Paper No. 92-GT-160, 1992

Launder, B.E.; Priddin, C.H.; Sharma, B.I.
"The Calculation of Turbulent Boundary Layers on Spinning and Curved Surfaces" Jorn. of Fluids Eng. Vol. 99, 1977

Launder, B.E., Sharma B.T.
"Application of the Energy Dissipation Model of Turbulence to the Calculation of Flow near a Spinning Disc" Lett Heat and Mass Transfer 1, 131-138, 1974

Rhie, C.M.
"A Numerical Study of the Flow past an Isolated Airfoil with Separation" Ph.D. Thesis, Dept. of Mechanical and Industrial Engineering, Univ. of Illinois at Urbana-Champaign, 1981

Rhie, C. M. and Chow, W.L.
"A Numerical Study of the Turbulent Flow past an Airfoil with Trailing Edge Separation" AIAA J1. 21 pp 1527-1532, 1983

Green, T., Turner, A.B.
"Ingestion into the Upstream Wheelspace of an Axial Turbine Stage" ASME-Paper No. 92-GT-303, 1992

Chew, J. W.
Prediction nf Flow in Rotating Disc Systems Using the k-ε Turbulence Model. ASME-paper 84-GT-229, 1984

Chew, J.W., Green, T., Turner, A.B.
"Rim Sealing of Rotor-Stator Wheelspaces in the Presence of External Flow" ASME-Paper No. 94-GT-126, 1994

Ko, S. H., Rhode, D. L. and Guo, Z.
"Computed Effects of Rim Seal Clearance and Cavity Width on Thermal Distributions" ASME-Paper No. 93-GT-419, 1993

Guo Z., Rhode D. L., Davis F. M.
"Cnmputed Eccentricity Effects on Turbine Rim Seals at Engine Conditions with Mainstream" ASME-Paper No. 94-GT-31, 1994

Sloan, D.G., Smith, P.J. and Smooth, L.D.
"Modelling of Swirl in Turbulent Flow Systems" Progress in Energy and Combustion Science, Pergamon Press Oxford, Vol 12 No. 3, 1986

Srinivasan, R. and Mongia, H.C.
"Numerical Computations of Swirling Recirculating Flow" NASA-CR 165197, 1980

Van Doormal, J.P. and Raithby, D.S.
"Enhancements of the SIMPLE Method for predicting incompressible fluid flows" Numer. Heat Transfer, 7 pp 147-163, 1984

Soo, S.L., Princeton, N.J.
"Laminar Flow over an Enclosed Disc" Trans. of the ASME, Paper 57-Sa-28, 1958

Owen, J. M., Rogers, R. H.
"Flow and Heat Transfer in Rotatiog Disc Systems" Vol 1, Research Studies Press Ltd, Taunton, Somerset, England, 1989

Dorfman, L. A.
"Effect of Radial Flow between Rntating Discs and Housing on their Resistance and Heat Transfer" Izv. Akad. Nauk-SSSR, OTN, Mekh i Mash, No.4, 26-32